Acta Cryst. (1977). A33, 268–276

Decomposition and Ordering in $Fe_{1-x}O$

BY B. ANDERSSON AND J. O. SLETNES

Institute of Physics, University of Oslo, Norway

(*Received* 22 *July* 1976; *accepted* 21 *September* 1976)

Samples in the composition range $Fe_{0.95}O$–$Fe_{0.88}O$ quenched from about 1000 °C, have been studied by electron diffraction/microscopy with special emphasis on the dark-field technique. The set of morphologies obtained by quenching and annealing confirms a spinodal-like decomposition in an oxygen-rich and an almost stoichiometric component. The diffraction spots and dark-field images reveal a considerable degree of order which is enhanced upon heat treatment below 300 °C. Previous diffraction studies have been interpreted in terms of an ordered phase with cubic symmetry. Dark-field microscopy, particularly at the symmetric composition, showed that the compositional fluctuation wave contained domains of tetragonal or orthorhombic symmetry at a very early stage. The range of order was found to increase during decomposition. An ordered phase of orthorhombic symmetry developed in oxygen-rich samples. Superstructure spots could be indexed by an *A*-faced orthorhombic cell with dimensions five times the fundamental cell. Extinctions lead to the space group *Abm*2 and a periodic antiphase relation. Only four types of clusters, all of which are based on three connected defect tetrahedra, are then possible.

1. Introduction

The phase $Fe_{1-x}O$ has a defect NaCl-type structure which is stable above 570 °C. The nonstoichiometry increases with increasing temperature and extends from $Fe_{0.95}O$ to $Fe_{0.88}O$ at 1000 °C. The presence of interstitial iron atoms as well as octahedral vacancies was established through neutron and X-ray studies by Roth (1960) and Smuts (1966). The concentrations were first determined accurately for quenched $Fe_{0.902}O$ by Koch & Cohen (1969) to 3·3% iron interstitials and 13.1% vacancies. From high-temperature measurements between 800 and 1200 °C Cheetman, Fender & Taylor (1971) found a ratio between vacancies and interstitials of about 3 to 4 for all compositions.

There is substantial evidence for clustering of these elementary defects in equilibrium (Kofstad & Hed, 1968; Koch & Cohen, 1969; Hayakawa, Morinaga & Cohen, 1974; Janowski, Jawoski & Benesch, 1973; Hoang, Romanov, Shayovich & Zvinchuk, 1973) as well as in the various metastable states which are obtained after quenching and heat treatment (Roth, 1960; Koch & Cohen, 1969; Hoang *et al.*, 1973).

The structure and ordered arrangement of these defect clusters appears to be less well known. From X-ray studies on one ordered structure near the phase boundary towards Fe_3O_4 Koch & Cohen (1969) and Hoang *et al.* (1973) both proposed a cubic structure based on clusters consisting of interstitials surrounded by vacancies. The proposals differ, however, both in regard to the cluster itself and the distance between clusters. From lattice images Iijima (1974) concluded that the clusters normally repeat with a monoclinic cell having unit vectors $\frac{5}{2}\mathbf{a}_c, \frac{5}{2}\mathbf{b}_c$ and $\frac{5}{2}\mathbf{c}+\frac{1}{2}\mathbf{a}_c$ where $\mathbf{a}_c, \mathbf{b}_c$ and $\mathbf{c}_c$ are the unit vectors of the NaCl structure. Other ordered structures have not been reported from diffraction studies although the existence of three subregions of wüstite has been suggested from thermodynamical studies by Vallet & Raccah (1966) and Fender & Riley (1969). However, lattice-parameter measurements at equilibrium temperatures (Hayakawa, Cohen & Reed, 1972) did not show the expected abrupt changes; neither do the main features of the scattering stemming from short-range ordering (Hayakawa, Morinaga & Cohen, 1974).

Upon quenching and subsequent heat treatment at temperatures below 570 °C the wüstite undergoes further ordering and below 320 °C a periodic decomposition into a stoichiometric and an iron-deficient component (Herai & Manenc, 1964; Herai, Thomas, Manenc & Bénard, 1964; Manenc, 1968; Hentschel, 1970). Manenc (1968) has described three low-temperature structures near $Fe_{0.88}O$ which he called *P'*, *P''* and *P'''*. *P'* corresponds to the equilibrium phase also studied by Koch & Cohen (1969) and Hoang *et al.* (1973). *P'*, which has an average periodicity of $2{\cdot}6a_c$, is found also as a constituent in the decomposed state resulting at higher iron content. *P''*, which is formed from *P'*, has an imperfect double periodicity of $5a_c$. *P'''*, which is formed by heat treatment at 500 °C, is still more ordered and yields sharp reflexions. Structure investigations of *P''* and *P'''* have not yet been reported.

The present investigation is aimed at a structure analysis of these superstructures. Particular attention is paid to the symmetry of the ordering since it is known from studies of other nonstoichiometric compounds like TiO and VO, that ordering of defects frequently leads to lower symmetry than that of the disordered parent matrix. Such transitions are often accompanied by very small distortions of the sublattice. Contributions from equivalent orientations of the same superstructure may then be difficult to distinguish by X-ray methods. The combination of electon diffraction and microscopy on the other hand, offers the relatively easy observation of the characteristic morphologies associated with structural changes and, in particular, the

possibility of identifying the origin of each reflexion through dark-field micrographs. Usually the unit cell and space group can be determined in this way, although a more complete structure analysis may depend generally on, for example, X-ray intensity data.

Consequently, an electron diffraction and microscopy investigation of the structure and morphology of wüstite in the whole composition range has been carried out. The samples were quenched from about 1000 °C and heat treated in order to study the different stages during ordering and composition variation.

The structure analysis has been concentrated on the ordered structure P'', which permits a more complete determination of the symmetry elements than the less ordered version P'.

2. Experimental

The samples were prepared from iron of purity 99·998 %. Foils of thickness about 1 mm were oxidized in an atmosphere of CO and CO_2 at 1000 °C and some at 900 °C. The compositions were predetermined by selecting partial pressures of CO and CO_2 as given by Darken & Gurry (1945). The samples were kept in equilibrium for some hours and then quenched by dropping them onto a cooled copper base, so that they reached room temperature in about a minute. The compositions were finally determined by measurement of weight gain during the process. The samples for heat treatment were encapsulated in evacuated silica tubes. The annealing time was chosen relatively short so as to prevent precipitation of Fe_3O_4 and Fe (Herai & Manenc, 1964). Fe_3O_4 was not observed except for a surface layer and some grains in the most iron-deficient samples.

Specimens were examined in a Philips EM 300 microscope equipped with goniometer stage. Suitable foils were obtained by mechanical polishing to a thickness of 0·1–0·2 mm followed by electrolytic polishing at about 1 V in phosphoric acid kept at 90 °C. Some specimens were finally ion-etched.

3. Results on decomposed samples

Over the whole composition range, the specimens produced by quenching and subsequent heat treatment display a sequence of morphologies which can be described in terms of a spinodal decomposition into an iron-deficient and a stoichiometric component as has been proposed previously by Anderson (1970) based on the results of Herai, Thomas, Manenc & Bénard (1964). Let us therefore arrange the results in composition regions corresponding to symmetric and asymmetric composition and to a nearly pure iron-deficient component.

3.1. *Compositions* $Fe_{0.95}O$–$Fe_{0.93}O$

Rapidly quenched samples of these compositions yield diffraction patterns (Fig. 1*b*) typical of P' structure: disc-shaped satellites around fundamental reflexions separated by $\delta\langle 100\rangle$; the distance δ corresponding to an average periodicity of about $2{\cdot}6a_c$. The shape corresponds to an ellipsoid approximately 15 Å wide and 25 Å long. The width is the same as Koch & Cohen (1969) measured under equilibrium conditions.

Dark-field images using the $\delta 20$ satellite (Fig. 1*a*) revealed small, random fluctuations with sizes consistent with the width of the satellite. The absence of any changes in the diffraction pattern suggests that the structure and morphology correspond closely to equilibrium state.

After heat treatment for 20 min at 300 °C satellite spots became sharper and additional spots appeared on corners, *e.g.* $\delta,2-\delta,0$. Dark-field images taken with superlattice reflexions (Fig. 2) exhibit a periodic decomposition structure on {100} planes, consistent with a three-dimensional network with period about 400 Å as reported by Herai, Thomas, Manenc & Bénard (1964) and Manenc (1968). The morphology is typical of a symmetric spinodal decomposition with {100} as the elastically soft planes in agreement with earlier investigations.

The width of the reflexions as well as the contrast of the oxygen-rich regions indicate a range of order appreciably shorter than the dimensions of the spinodal decomposition waves. The dimensions of the fluctuations are about twice that of the quenched state with the longest dimension apparently aligned along the line of compositional maxima.

Each set of compositional waves was found to appear in dark-field images using any superlattice reflexion. It was therefore concluded that the reciprocal unit cell was $\delta\times\delta\times\delta$ as proposed before. However, the contrast of one set of waves can be enhanced with a particular reflexion. For instance, by using the $\delta 20$ reflexion, [010] waves are outlined (Fig. 2*b*). The satellite $\delta 20$ thus receives a larger contribution from the ordering within these waves than from the other, [100] or [001] waves. The symmetry must therefore be tetragonal or orthorhombic as would be expected also from the shape of the ordered P'-type regions. The model for the morphology in the orthorhombic case is shown schematically in Fig. 1(*e*).

3.2 *Compositions around* $Fe_{0.92}O$

In this composition range, the original state could not be retained after the same rapid quenching as for $\sim Fe_{0.94}O$ samples. This indicates the process to be more rapid as would in fact be expected for an asymmetric spinodal decomposition.

Dark-field images of quenched samples (Fig. 3) reveal that the iron-deficient component is found in regions of dimensions about 1000–4000 Å which are extended in ⟨100⟩ directions. This is a typical morphology for asymmetric spinodal decomposition. Decomposition on a smaller scale could not be identified. The regions appear ordered but heavily faulted. In agreement with this the diffraction patterns (Fig. 3*a*) show sharper reflexions than for $\sim Fe_{0.94}O$, a relatively

higher intensity of reflexions like $\delta,h-\delta,0$ and also secondary satellites. The dark-field images again show the symmetry to be either tetragonal or orthorhombic.

3.3. *Compositions less than* $Fe_{0.91}O$

At compositions in this range, the decomposition was found to proceed even faster. After quenching, a coarsened state was normally obtained in which the more ordered structure P'' was formed (Fig. 5).

A particularly fast-quenched sample with composition $Fe_{0.891}O$ revealed a morphology corresponding to an earlier stage, *i.e.* the asymmetric spinodal (Fig. 4). The proportion of the iron-rich component is apparently very small. A tendency for the double period of P'' is present even in P' as indicated by diffuse scattering between the satellite spots (Fig. 4*a*).

The reciprocal lattices of P' and P'' are closely related (Fig. 6). The P' reflexions are found on a cubic lattice with parameter $\delta a_c^* = 1/2{\cdot}6 a_c$ while the strong superlattice spots of P'' are positioned on a cubic lattice with the parameter slightly changed to $\Delta a_c^* = \frac{2}{5} a_c^*$. In addition, streaked reflexions appear on edges and face centres of the cube, and also faint ones in the body centre $\Delta/2,\Delta/2,\Delta/2$. Diffraction patterns taken from the quenched state reveal the two lattice types simultaneously (Fig. 5*c*, *d*).

Dark-field images from the two structures can be obtained separately (Fig. 5*a*,*b*), which reveal a homogeneous precipitation of P'' inside P'. No special shape or distribution of P''-type crystal grain was noticed.

4. Ordered phase

4.1. *Reciprocal lattice*

Specimens of composition $Fe_{0.89}O$ were selected for analysis of the P'' structure. After heat treatment for 30 min at 225°C the original P' structure had transformed completely to P''. The reciprocal lattice and diffraction symmetry were determined from selected-area diffraction patterns and a large number of dark-field images. The observations could be explained by an A-faced orthorhombic cell with cell parameters not observably different from $5a_c$ and with the following extinctions: hkl: $k+l=2n+1$; $0kl$: $k(l)=2n+1$. These two rules lead unequivocally to space group $Abm2$ (No. 39). A third rule hkl: $k+l/5=2n+1$ is also found. This is clearly an accidental one and will be discussed below.

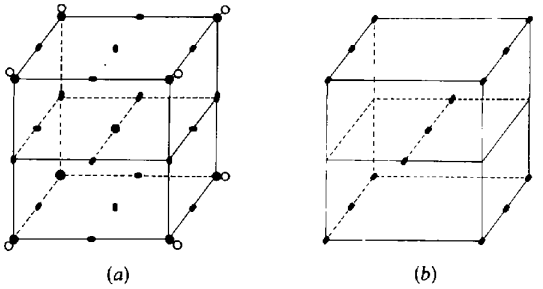

(*a*) (*b*)

Fig. 6. (*a*) A repetition unit in reciprocal space for P' and P'' structures. The sizes of the cubic cells are $\Delta = 1/2{\cdot}5$ and $\delta \simeq 1/2{\cdot}6$ measured in fractional indices. (*b*) The single-crystal diffraction pattern. The reflexions are shown elongated in the orthorhombic [100] direction.

Single-crystal patterns are shown in Fig. 7(*a*) for layers $h0l$, $h1l$ and $h2l$. The extinguished reflexions appear for odd h where $l=0,10$ and for even h where $l=5$ (rule 3). Only those with l odd are present in $h1l$ (rule 2).

A superposition of six equivalent patterns, which can be compared with the observed diffraction patterns (Figs. 8, 9 and 10), is shown in Fig. 7(*b*) for layers h_ck_c0, $h_ck_c\Delta/2$ and $h_ck_c\Delta$. The second rule is still effective and can be written h_ck_c0: $h_c(k_c)=(2n+1)/2$. Reflexions from crystals with a and b interchanged will overlap. As indicated in Fig. 7(*b*), extinctions due to the third rule will therefore appear only for rows $\langle h,5n,5n'\rangle$ which pass through subcell reflexions.

Fe_3O_4 reflexions from the coherent surface layer are also present. These are surrounded by satellites of the same type as around 200_c *etc.* By tilting the specimen, these satellites can be shown to arise through multiple scattering. Some very faint streaks around positions separated by $\Delta/2[100]$ *etc.* from the sublattice reflexion (Fig. 8) could also be shown, by tilting experiments, to result from double diffraction.

The equivalent orientations of the orthorhombic unit cell produce very similar diffraction patterns as may be seen from Fig. 7. For this reason a large number of dark-field pictures were needed to ascertain the origin of the different reflexions. The extinction rules then followed from the reflexions which receive some contribution from only one – or none – set of domains. A summary of these observations is given below.

Reflexions with contributions from all six orientations were found on the corners and body-centre of the repetition cube shown in Fig. 6, *i.e.* reflexions with indices all even or all odd. The reflexions are characterized by the complex contrast in dark-field images (Fig. 11*c*) indicating several contributions.

Most of the streaked reflexions on the edges and face-centres of the cube (Fig. 6) with mixed odd and even indices received only two contributions, as was indicated by the fringed contrast in the corresponding dark-field images, related to frequent planar faults in the [100] direction.

Closer inspection of the streaked reflexions revealed that all those in layers where h_c, k_c or l_c is a whole number, have only one contribution. For instance in h_ck_c0 a domain structure (Fig. 11*a*) appeared in dark field from reflexions streaked in the same direction. The planar [100] faults here aided the identification of domain orientation. Reflexions streaked in another direction revealed a second domain orientation (Fig. 11*b*). The reciprocal unit in the (001) reciprocal plane is by vector addition $\Delta/2\mathbf{a}_c^* + \Delta\mathbf{b}_c^*$.

The domains observed for $l_c=0$, are also imaged for

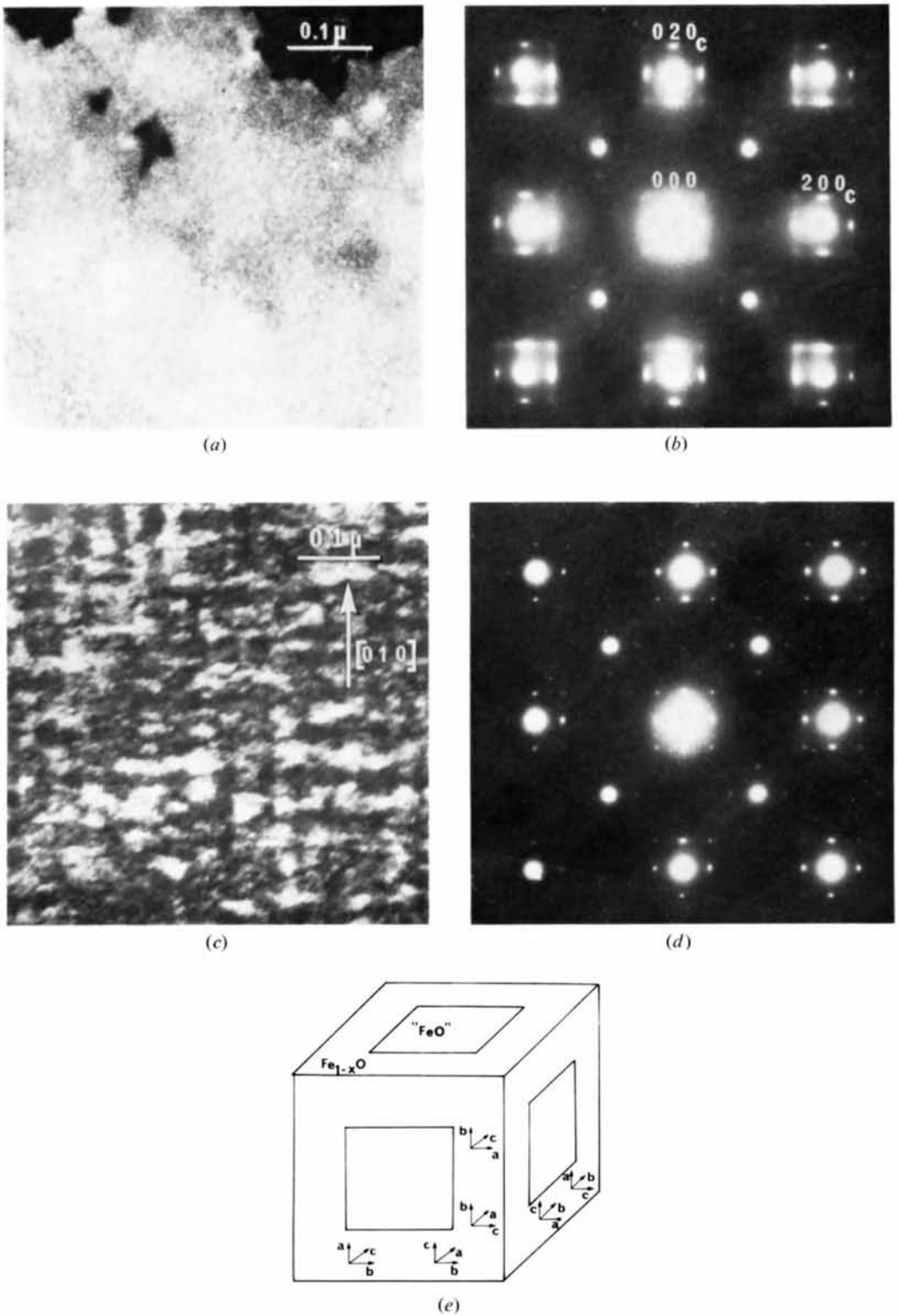

(a) (b) (c) (d) (e)

Fig. 1. $Fe_{0.939}O$: (*a*) dark-field image formed by satellite $\delta 20$ of a rapidly quenched sample; (*b*) the (001) diffraction pattern, (*c*) and (*d*) are the same images taken after heat treatment for 20 min at 300 °C, (*e*) The proposed distribution of domain orientations in each compositional wave.

[*To face p.* 270

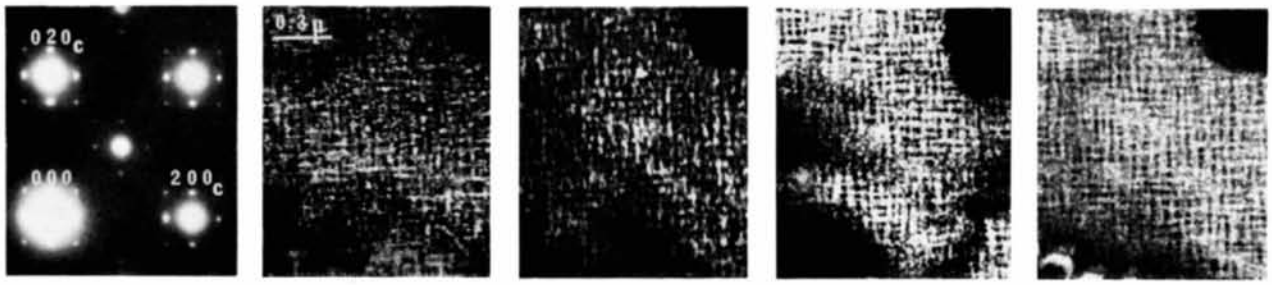

(*a*) (*b*) (*c*) (*d*) (*e*)

Fig. 2. Dark field images from heat-treated $Fe_{0.939}O$: (*a*) the (001) diffraction pattern, (*b*) images formed by $\delta 20$, (*c*) by $0,2-\delta,0$, (*d*) by 02δ and (*e*) by $\delta,2-\delta,0$.

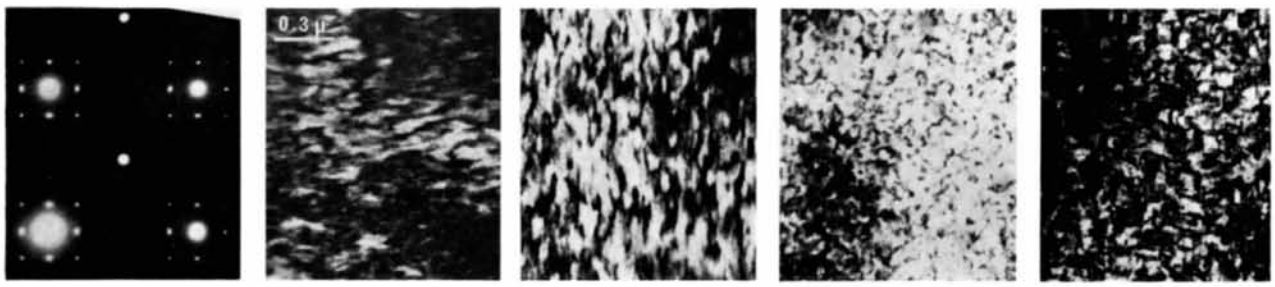

(*a*) (*b*) (*c*) (*d*) (*e*)

Fig. 3. Dark-field images from quenched $Fe_{0.921}O$. (*a*)–(*e*). Conditions as in Fig. 2.

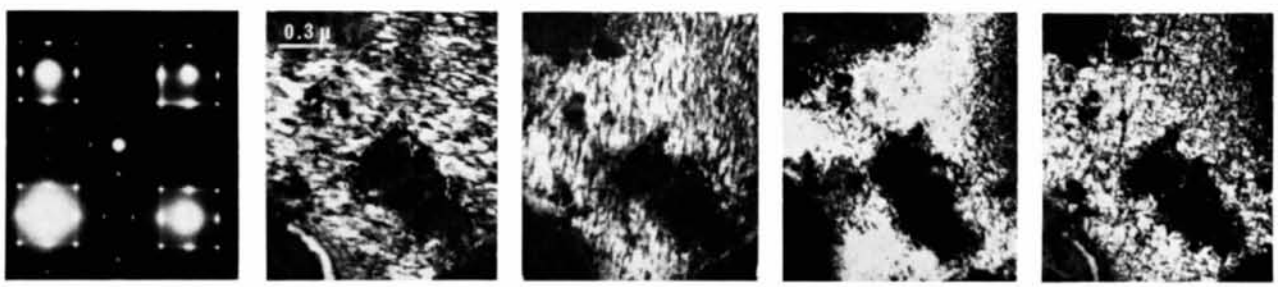

(*a*) (*b*) (*c*) (*d*) (*e*)

Fig. 4. Dark-field images from quenched $Fe_{0.891}O$. (*a*)–(*e*). Conditions as in Fig. 2.

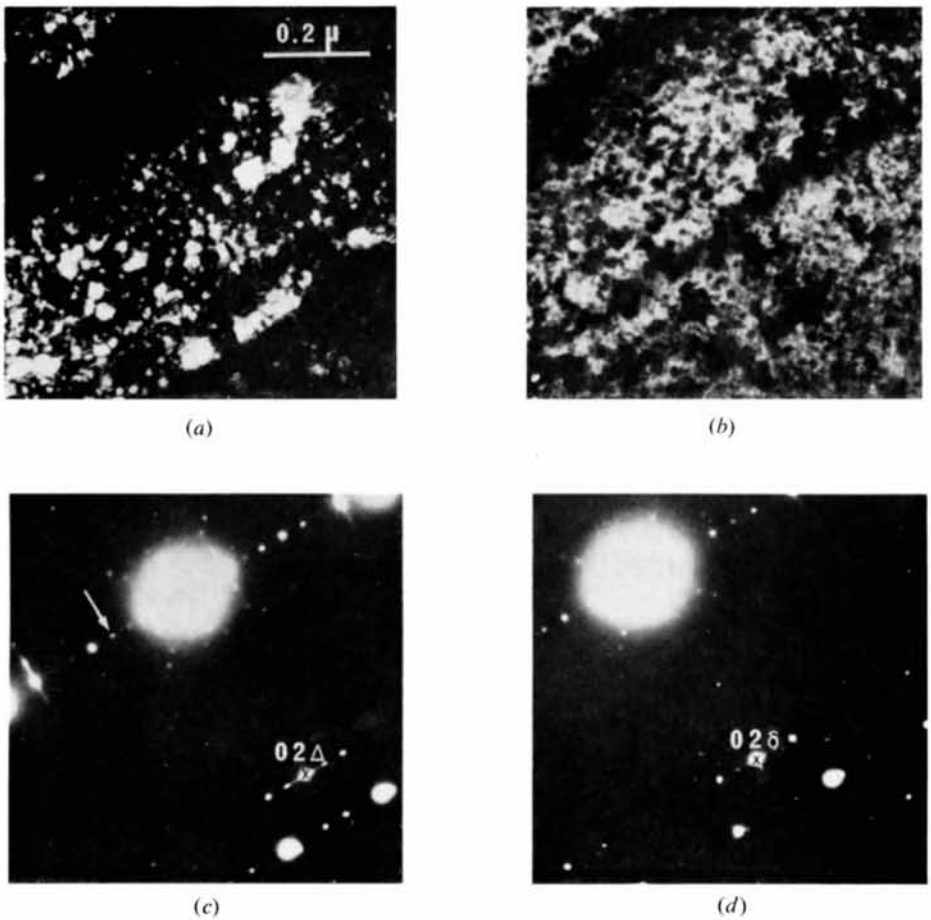

(a) (b)

(c) (d)

Fig. 5. Quenched $Fe_{0.897}O$. Dark-field images, formed by indicated reflexions, display precipitates of P'' in P' phase. Diffraction spots are split into an integer and a non-integer reflexion.

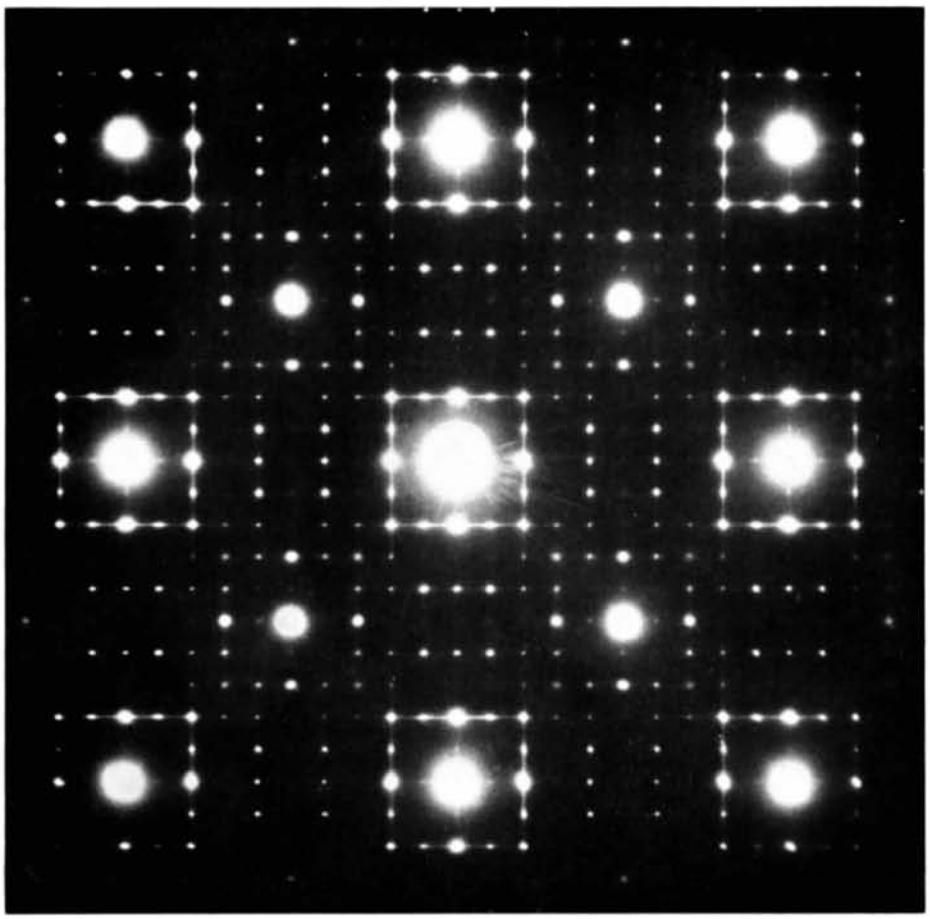

Fig. 8. The $(001)_c$ diffraction pattern, *cf.* the schematic representation at the top of Fig. 7. The streaked reflexions corresponding to a periodicity of $5a_c$, receive contributions from the two domain orientations shown in Fig. 7 (*a*) and (*b*).

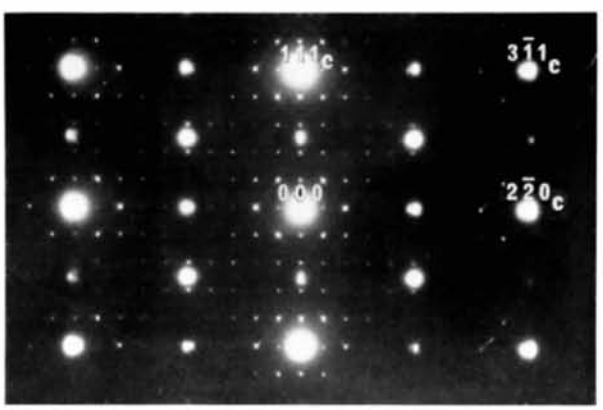

Fig. 9. $(1\bar{1}2)_c$ diffraction pattern of the P'' structure. Indices refer to the NaCl-type cell.

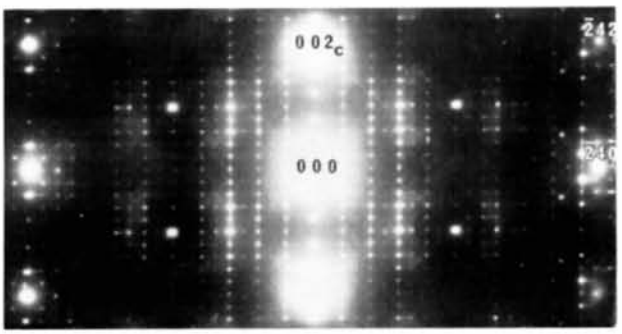

Fig. 10. (210) diffraction pattern of the P'' structure.

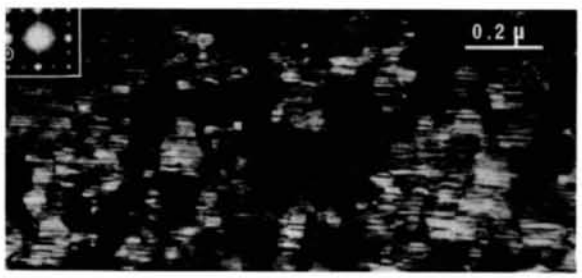

(*a*)

(*b*)

(*c*)

Fig. 11. Dark-field images from reflexions (*a*) $\Delta,2-\Delta/2,0$, (*b*) $\Delta/2,2-\Delta,0$ and (*c*) $\Delta,2-\Delta,0$, corresponding to 290, 180 and 280. Inset: The positions of the reflexions. In (*a*) and (*b*) the *a* axis is normal to and the *c* axis parallel to the faults and the common *b* axis is normal to the image plane.

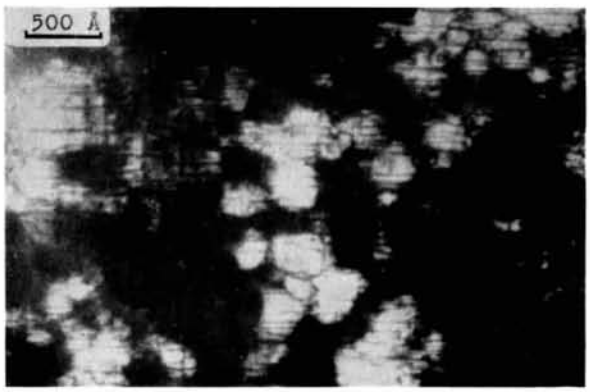

(*a*)

(*b*)

Fig. 12. Faults in a dark-field image (*a*) visible as dark regions and in a lattice image, (*b*) seen to be subdivisions of the larger (5x) period and probably narrow regions of different orientation.

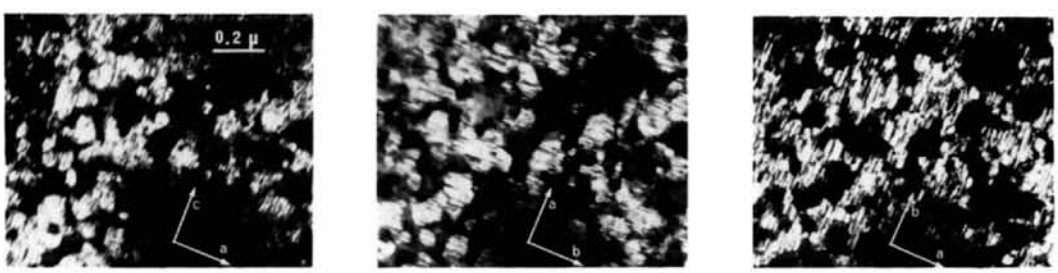

(*a*) (*b*) (*c*)

Fig. 13. Dark-field images from (*a*) $\Delta/2,2,\Delta$ (*b*) $\Delta/2,2-\Delta,0$ and (*c*) $\Delta,2-\Delta/2,0$ corresponding to reflexions 1,10,2, 180 and 290 which receive intensity from one domain orientation. The directions of the axes in the imaged domains are indicated in the figures.

$l_c=1$. This was established by comparing satellites to 000 and 111_c in the $(11\bar{2})_c$ reciprocal plane (Fig. 9) and also satellites to 002_c and 131_c in the $(3\bar{1}0)_c$ reciprocal plane. Reflexions having one contribution therefore repeat in the third direction with the sublattice, *i.e.* $\mathbf{a}^*_c+\mathbf{b}^*_c+\mathbf{c}^*_c$ or the equivalent $\Delta/2\mathbf{a}^*_c+\mathbf{c}^*_c$.

Since all domains generally contribute to reflexions belonging to the $\Delta\times\Delta\times\Delta$ unit the unit vectors are $\Delta/2\mathbf{a}^*_c$, $\Delta\mathbf{b}^*_c$, $\Delta\mathbf{b}^*_c+\Delta\mathbf{c}^*_c$ which corresponds to an A-centred orthorhombic Bravais lattice with $a=b=c=5a_c$. Alternatively one could use the positions of the reflexions having two contributions to arrive at the same conclusion about the third axis.

The third extinction rule follows directly from the positions of reflexions having one contribution. The Bravais lattice is namely invariant to an interchange of the b and c axes, and streaked reflexions should have two contributions unless one is extinguished.

The second rule affects both domain orientations. The corresponding spots are therefore not observed, as multiple scattering to the positions is not possible in the $l_c=0$ layer.

4.2. *Morphology*

The domains do not show any special shape but have frequent planar [100] faults. In a lattice image (Fig. 12) the faults appear as regions of shorter periodicity. Linear faults are also present as starting points for subdivisions inside a domain.

The relative distribution of domains is not arbitrary. Referring to the dark-field picture reproduced in Fig. 11(*a*) and (*b*), the two sets of domains with a common b axis are seen to be almost complementary. To specify the orientation of a domain we may keep the cube axes fixed as a reference system and specify the domain orientation by for instance [*abc*] where the

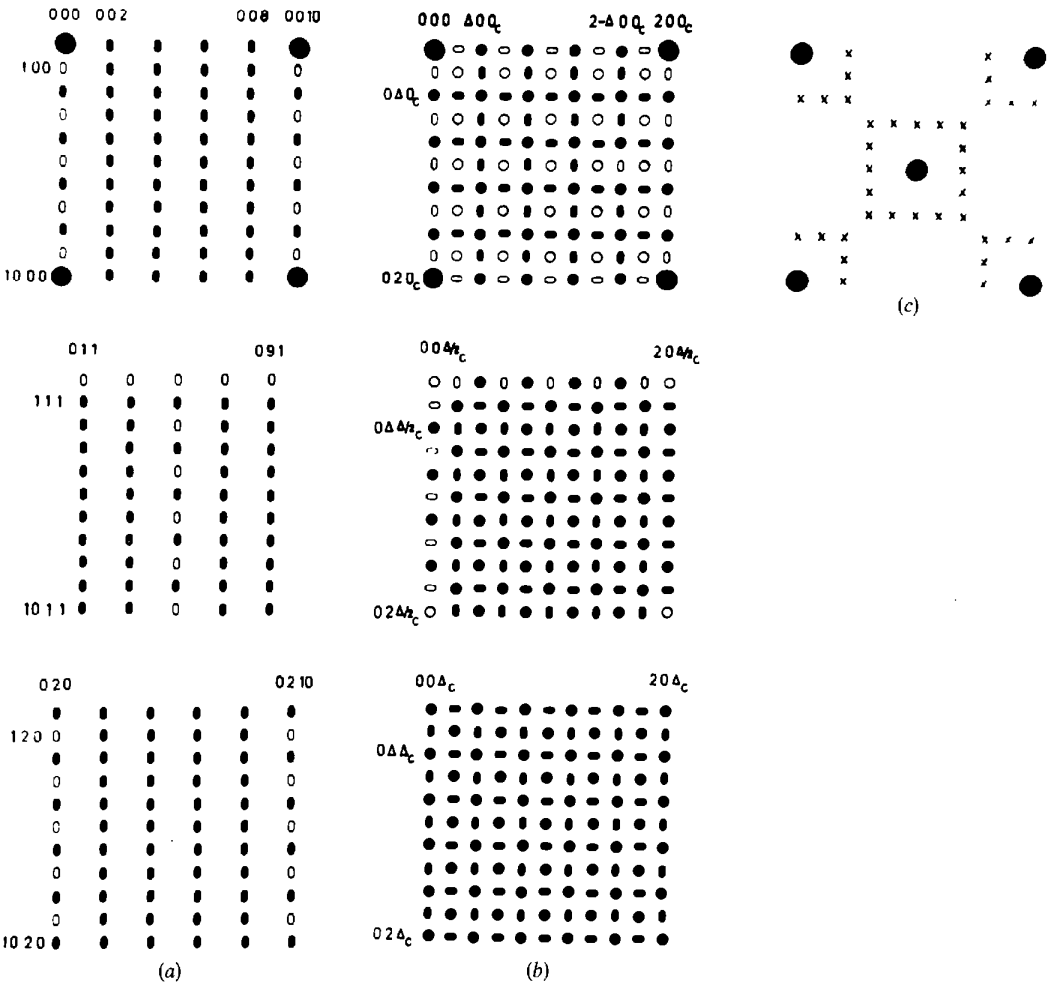

Fig. 7. (*a*) A schematic representation of the reciprocal lattice of the P'' structure in layers $h0l$, $h1l$ and $h2l$. Extinguished reflexions are shown open. (*b*) The corresponding layers h_ck_c0, $h_ck_c\Delta/2$ and $h_ck_c\Delta$ where contributions from all six orientations are added. (*c*) The diffraction pattern of Fe_3O_4 together with the position of double diffracted satellites marked by crosses.

orthorhombic axes a, b and c are pointing along $\mathbf{a}_c$, $\mathbf{b}_c$ and $\mathbf{c}_c$ respectively.

The complimentary domains viewed in Fig. 11(*a*) and (*b*) are thence [*abc*] and [*cba*]. Continuing with [*acb*] domains which are imaged by the $\Delta/2,2_c,\Delta$ reflexion, these have common a axes with [*abc*] and again are found in nearly complementary areas (Fig. 13). Also domains with a common c axis are complementary. Thus domains [*bac*], [*acb*] and [*cba*] have nearly the same projection and [*abc*], [*bca*] and [*cab*] are the complementary areas. There is thus one set of domains where the axes are permutations of [*abc*] with a fixed sequence and another set which is identical, only inverted.

4.3. *Structure analysis*

Through the present electron diffraction and microscopy study the unit cell, space group and an accidental extinction rule are established. Let us now attempt to derive a structure model which is consistent with this new information as well as other available information about composition, existence of vacancy–interstitial clusters and previously measured X-ray intensities.

The analysis will start with a discussion of the third rule. This rule indicates an additional symmetry operation in the structure. The nature of this operation may be seen from a structure factor contribution $1+\exp[2\pi i(hx+ky+lz)]$ from atoms separated through $[xyz]$. This expression has the required zeros, for $h+l/5=2n+1$, if $[xyz]=[\frac{1}{2},0,1/10]$, *i.e.* a periodic antiphase relation with $M=2{\cdot}5a_c$ and a shift vector $\frac{1}{2}\mathbf{a}_c$ along $\mathbf{c}$. Such a shift will preserve the fundamental NaCl-type structure.

In the original cubic structure the antiphase period can develop along the three cubic directions. For each of these directions there are two possible shift vectors. The unit cell is the same, but the direction determines the extinctions so that domains with different shift vectors can be distinguished.

Previous investigations have established the tendency for clustering. Since the space group *Abm*2 contains four- and eightfold positions and taking into account the periodic antiphase relation, the atoms, as well as the clusters, will have to be positioned in multiples of eight or sixteen.

If all defects are bound to eight clusters, the closest ideal number is found to be ten iron vacancies (V_m) and three iron interstitials (M_i) which gives the vacancy to interstitial ratio 3·3 and the formula $Fe_{444}O_{500}$ which is in good agreement with reports of the observed single-phase compositions $Fe_{0\cdot902}O$, $Fe_{0\cdot88}O$ and $Fe_{0\cdot87}O$ of P' phase. An increase to the next possible ideal number, $13V_m+4M_i$ as in the Koch & Cohen (1969) type of cluster, leads to the composition $Fe_{0\cdot856}O$ which is outside the range of P'-phase. It is then necessary to have a non-ideal occupancy number to make up for the discrepancy in compositions as no decomposition has been observed in connexion with the transition to P''. The same problem arises with 16 clusters in a unit cell. Besides, this appears to be less probable as the cluster size approaches that of a single defect tetrahedron.

Hence $10V_m+3M_i$ is the most likely cluster size and therefore primarily considered. Let us further retain the assumption from previous work that the metal interstitials are surrounded by vacancies. The clusters thus consist of defect tetrahedra with one interstitial surrounded by four vacancies on the nearest octahedral sites.

One of the interstitials in a cluster must occupy a special position of which there are three in space group *Abm*2, denoted 4(*a*), (*b*) and (*c*). For tetrahedral sites only 4(*a*) and (*b*), positioned on the twofold axes $0,0,z$ and $\frac{1}{2},0,z$, are available as 4(*c*) positions are on (010) mirror planes. Letting four interstitials, which are also the centres of the clusters, be in 4(*a*) with $z=0$, then four other interstitials must be in 4(*b*) with $z=0{\cdot}1$ owing to the periodic antiphase relation. Other choices of the z component, keeping the sublattices of the NaCl structure fixed, will lead to the same structure.

The clusters can be classified by the vector $[xyz]$ from the central interstitial to another interstitial. The third interstitial will then appear at $[\bar{x}\bar{y}z]$ because of the twofold axis. The vacancies can be placed in eightfold positions so as to form the defect tetrahedra. For the separations $\frac{1}{2}\langle 110\rangle_c$ and $\frac{1}{2}\langle 111\rangle_c$ the tetrahedra will share corners and thus have the required size $10V_m+3M_i$. In the first case all tetrahedra have the same orientation, and in the second case the outer two and the central one will appear with opposite orientations. For the separation $\frac{1}{2}\langle 100\rangle_c$ the tetrahedra share edges, leaving two vacancies to be positioned outside the tetrahedra. Larger vectors will separate the clusters so that tetrahedral units appear.

The central tetrahedra have sites around the lattice points. The outer two can be connected to the central one in nonequivalent ways with respect to the orthorhombic axes. Thus for $\frac{1}{2}\langle 100\rangle_c$ there are three possibilities, for $\frac{1}{2}\langle 110\rangle_c$ also three and for $\frac{1}{2}\langle 111\rangle_c$ one – in all seven structure models. There will be one type of cluster for separation $\frac{1}{2}\langle 100\rangle_c$, two for $\frac{1}{2}\langle 110\rangle_c$ and one for $\frac{1}{2}\langle 111\rangle_c$ (Fig. 14*a*). The last structure model is shown in Fig. 14(*b*).

The selection of the correct model has been attempted on the basis of X-ray intensity measurements reported by Koch & Cohen (1969). Calculated intensities must in this case be added for the six orientations of the orthorhombic cell, however, and difficulties in distinguishing the different models are considerable. From the reflexions measured by Mo rays the R value becomes 0·36 for the model with separation $\frac{1}{2}\langle 111\rangle_c$, 0·38–0·39 for $\frac{1}{2}\langle 110\rangle_c$ and 0·40–0·42 for $\frac{1}{2}\langle 100\rangle_c$ when no displacements are considered. The values can be compared with $R=0{\cdot}62$ obtained by Koch & Cohen for their model without displacements. As indicated by the small differences in R, the values for the average structure factor show only small variations from one model to another; typically a few tenths on the scale

used by Koch & Cohen (1969) (Table 1). Since changes expected from adjustment of atomic positions are several times larger, the correct model cannot be selected. This is also reflected in the Patterson maps, which are nearly identical for the models. Reasonable agreement with experimental maps was noticed.

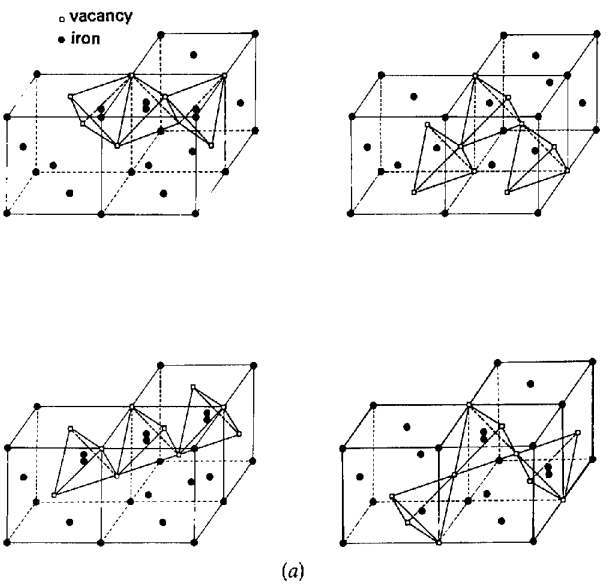

(*a*)

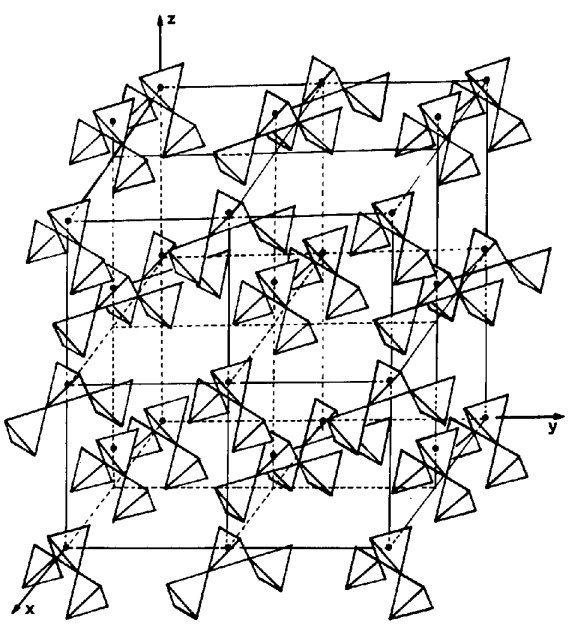

(*b*)

Fig. 14. (*a*) Possible models for the cluster; one for the distance $\frac{1}{2}\langle 100\rangle_c$ between interstitials, two for $\frac{1}{2}\langle 110\rangle_c$ and one for $\frac{1}{2}\langle 111\rangle_c$. (*b*) Structure model for *P*″ or $Fe_{444}O_{500}$ using the $\frac{1}{2}\langle 111\rangle_c$ type of cluster. Only the defect clusters are shown. The dots indicate the lattice points in the unit cell.

Table 1. *Observed and calculated structure factors*

F_{calc} is the square root of the sum of intensity contributions from the six orientations; F_{obs} is from Koch & Cohen (1969).

h	*k*	*l*	F_{obs}	F_{calc}	*h*	*k*	*l*	F_{obs}	F_{calc}
0	0	2	0·60*	3·28	13	5	15	4·14	4·58
0	0	4	0·60*	3·03	15	5	23	4·22	4·18
0	0	6	0·60*	2·50	13	5	25	2·68	2·98
0	0	8	10·95	9·03	13	5	23	0·95	0·58
0	0	14	0·60*	1·01	15	5	33	3·94	3·52
0	0	16	1·51	2·75	13	5	35	1·70	1·99
0	0	18	4·37	4·80	15	5	43	3·36	2·82
0	2	20	1·75	1·77	15	5	53	2·09	2·06
0	0	22	1·73	1·70	15	13	15	3·31	3·60
0	0	28	5·32	5·33	15	15	23	3·54	3·51
2	0	30	2·17	2·04	13	15	23	0·87	0·32
0	0	32	1·22	1·12	15	15	33	3·40	3·09
0	0	38	2·63	3·07	13	15	35	1·53	1·78
2	0	40	1·22	1·04	15	15	43	2·75	2·51
0	0	42	1·22	1·42	18	0	30	3·11	2·69
0	0	48	2·98	3·09	20	0	28	4·14	3·93
2	0	50	0·98	1·22	20	0	38	2·34	2·41
5	5	3	3·94	5·58	18	0	40	1·64	1·46
5	3	3	1·34	1·03	20	0	48	2·15	2·50
5	5	13	5·59	6·32	18	10	20	3·78	3·55
5	5	23	5·48	5·17	18	10	18	0·75	0·58
3	5	25	2·06	2·36	20	10	28	2·13	2·80
3	5	23	1·56	0·62	20	10	38	3·09	2·69
5	5	33	4·66	4·07	20	20	28	1·66	3·11
5	5	43	3·70	3·19	20	20	38	1·96	1·93
5	5	53	2·33	2·32	20	20	48	1·25	2·03
10	0	18	6·57	5·34	25	5	33	3·76	2·72
8	0	20	2·61	4·75	23	5	35	2·02	2·08
8	0	30	2·26	2·07	25	5	43	2·54	2·23
10	0	28	5·89	3·75	23	15	25	2·33	2·64
8	0	40	1·93	2·19	25	15	33	2·81	2·42
10	0	38	1·11	3·38	23	15	35	1·94	1·87
10	8	10	6·56	5·50	23	25	25	2·02	2·09
8	10	20	1·87	2·82	25	25	33	2·03	1·93
8	10	18	0·60*	0·81	25	25	43	1·45	1·59
10	10	28	4·13	4·12	33	5	35	2·25	1·91
8	10	30	2·08	2·61	35	5	43	1·56	1·57
8	10	28	1·14	0·52	33	5	45	1·04	1·22
8	8	30	1·87	0·68	33	15	35	1·66	1·72
10	10	38	2·28	2·40	33	25	35	1·24	1·40
8	10	40	1·39	1·43	35	23	35	0·81	1·13

* Not detected.

To show the agreement with available data, a comparison has been made in Table 1. Structure factors for only one model are shown as the variations are small. The model with separations $\frac{1}{2}\langle 111\rangle_c$ between interstitials is chosen since the *R* value was found to be lowest. For this model, when estimated displacements are incorporated, an *R* of 0·17 was obtained. The list of parameters with displacements is shown in Table 2. No refinement was performed as the number of adjustable parameters is very large and the uncertainties connected with the effects of several crystal orientations and of crystal imperfection is large. The *R* value is, however, about the same as Koch & Cohen (1969) obtained for their refined model.

5. Discussion

Through the present study, we have shown that the unit cell of *P*″, a metastable ordered wüstite of compo-

sition $\sim Fe_{0.89}O$ obtained by heat treatment, to be orthorhombic with $a=b=c=5a_c$. This differs from previous proposals but agrees well with Iijima's (1974) electron-microscope investigation on P' structure since the P'' structure projected along the $\langle 100\rangle_c$ directions will appear as periodic twins of the monoclinic cell which he proposed. The numerous untwinned regions thus correspond to faults in the periodic antiphasing in the P'' structure. It also becomes evident that the P' and P'' structures appear identical except for such planar faults and faults in periodicity. The P' structure can therefore be taken as orthorhombic.

Table 2. *Atomic positions* ($\times 10^3$) *in the* $\frac{1}{2}\langle 111\rangle_c$*-structure model*

x	y	z
4 Interstitial Fe in 4(*a*)		
0	0	50
4 Interstitial Fe in 4(*b*)		
500	0	150
8 Interstitial Fe in 8(*d*)		
100	100	−50
8 Interstitial Fe in 8(*d*)		
600	100	50
80 Vacancies in 8(*d*)		
50	50	0
650	50	0
150	150	0
550	150	0
−50	50	100
550	50	100
650	150	100
450	50	200
850	50	400
950	150	400
100 Octahedral Fe in 4(*c*)		
50	250	0
247	250	0
453	250	0
645	250	5
850	250	0
−50	250	100
150	250	97
350	250	100
550	250	100
747	250	100
50	250	200
250	250	200
450	250	200
650	250	197
850	250	200
−50	250	300
150	250	300
350	250	300
550	250	300
50	250	−197
−47	250	−100
250	250	400
550	250	−97
650	250	400
145	250	−95
320 Octahedral Fe in 8(*d*)		
747	−47	0
455	45	5
145	−45	0
350	150	0
745	145	5
−45	145	0
145	55	95
645	−45	100
747	50	100
55	145	95
247	150	97
455	145	100
147	−147	100
45	45	195
250	50	200
645	55	195
148	0	198
148	148	198
647	−147	200
555	145	195
747	150	197
−50	147	198
55	55	−195
150	50	300
648	0	298
545	45	295
247	50	−197
247	250	−197
250	150	300
450	147	298
648	148	298
145	145	195
−45	45	−95
747	50	−97
555	55	−95
650	50	400
150	150	400
645	145	295
747	250	−97
245	145	−95
100 Octahedral O in 4(*c*)		
50	250	−100
250	250	−100
450	250	−100
650	250	−100
850	250	−100
−50	250	0
150	250	0
350	250	0
550	250	0
750	250	0
50	250	100
250	250	100
450	250	100
650	250	100
850	250	100
−50	250	200
150	250	200
350	250	200
550	250	200
750	250	200
50	250	300
250	250	300
450	250	300
650	250	300
850	250	300
400 Octahedral O in 8(*d*)		
47	47	−103
253	50	−100
450	50	−100
650	50	−103
−53	150	−100
153	153	−103
350	150	−100
550	150	−103
750	150	−100
150	−53	−100
54	−54	−4
154	46	4
447	150	0
547	47	−3
753	50	0
46	154	4
253	150	0
650	−53	0
653	153	−3
850	150	0
54	54	104
250	50	100
554	−54	96
654	46	104
−50	153	103
153	153	103
350	150	100
546	154	104
753	150	100
153	−50	103
−50	50	203
46	153	202
450	153	203
554	54	204
750	50	200
153	46	202
250	150	200
653	−50	203
653	153	203
850	150	200
50	50	300
250	50	300
450	50	303
546	153	302
150	50	−203
150	150	300
350	150	300
653	46	302
750	150	300
50	150	−203

The ordering of defects is associated with the P' structure throughout the studied composition range. The changes of this structure are remarkably small, *viz* a decrease in average periodicity from 2·74 to 2·60 and an increase in the range of order for quenched samples but not when held at high temperatures (Hayakawa *et al.*, 1974). The authors explained the invariance of the structure by assuming variations in the cluster size. It can also be seen as indicative of varying concentrations of local regions enriched in defects.

The close relation found between the quenched state of $Fe_{0.939}O$ and the equilibrium state is of particular interest in this connexion. With the observation of the mottled contrast in dark-field images (Fig. 1*a*) as a starting point, the existence of quite distinct composition fluctuations forming small elongated regions of orthorhombic symmetry may then be suggested in the equilibrium state.

This way of describing the state can incorporate the existence of subregions as suggested by Vallet & Raccah (1965) by supposing that changes in the size and distribution of ordered regions can take place in such a way as to produce morphological changes throughout the samples with characteristics approaching a phase transition. The subregions would then be associated with the size of composition fluctuations, which is governed by the average composition as well as temperature. Since the morphological changes are on a very small scale, ~20 Å, the changes may in a sense be looked upon as differences in the short-range-order structure. Such changes may not necessarily be followed by abrupt changes in lattice parameter or in the main features of the diffuse scattering.

Decomposition in the metastable state takes place both on this local scale involving ordering and on a larger scale with characteristics typical of a spinodal decomposition. A binary solution cannot be unstable to both short and long decomposition waves in the original formulation of the theory for spinodal decomposition (Cahn, 1968). This may be possible, however, if local order is introduced as an extra parameter. Also, the extension to the ternary case should be considered since metal atoms, vacancies and interstitials take part in the diffusion. The results have therefore been compared with a calculation by Morral & Cahn (1971) for such a system. It is found that in one of the three cases sketched by these authors an instability to fluctuation waves below a certain value corresponding to ordering was shown to exist. This limiting value increases when the temperature is lowered. At a critical temperature the ternary solution is shown to be unstable to long waves as well, giving rise to spinodal decomposition with a morphology closely related to the binary case. The present observations agree well with this behaviour but further investigation, especially of the time development, will be necessary to decide whether the decomposition is really of spinodal type or not.

The ordering seems to proceed preferentially along the direction defined by the composition maxima of the spinodal waves. Since the domains with this axis pointing along $[100]_c$ and $[010]_c$ contribute most to $\delta 20_c$ and $0,2-\delta,0_c$, respectively, the axis can be determined if the structure factors are known. The calculation of the contributions to $0,2-\delta,0_c$ based on the P''-structure (Table 2) indicate that the preferred direction of ordering is along **b** but this is not confirmed by calculation on the $\delta 20$ reflexion.

Minimization of the elastic energy seems to be an important factor in determining the characteristic morphology. For instance, at composition $Fe_{0.939}O$ the compressive stresses on the waves will favour the formation of ordered regions having the longest axis pointing along the direction defined by the composition maxima. One axis larger than the others may therefore explain the existence of two domain orientations with a common axis within each wave. The complementarity of these domains is possibly carried over in the morphology of the P'' structure. In addition, there are relations between other neighbouring domains, governed probably by elasticity although minimization of the interfacial energy may play an important part. The discussion of the morphology can not be carried far since detailed lattice relations between neighbouring domains have not been determined.

Regarding the structure of P'' the positions of the clusters could be determined uniquely, and a preferable cluster size of ten vacancies and three interstitials was found. If the interstitials are completely surrounded by vacancies, the cluster consists of three defect tetrahedra sharing corners or, alternatively, edges if free vacancies are allowed. The point symmetry of the cluster limits the number of types to four and the number of structure models to seven. A structure analysis to distinguish models was found to be futile on the basis of existing structure factor data since these receive several contributions. When contributions for all six orientations are added, the resulting structure factors differ little from one model to the next, and in fact also differ little from results based on the Koch & Cohen (1969) type of cluster. This illustrates that the models, when averaged over orientations, are very similar and in fact closely related to the Koch & Cohen (1969) type of cluster.

To distinguish the models some information about single crystals is needed. The domains may be grown somewhat larger but the size necessary for X-ray experiments is hardly attainable. However, the streaked, double-period reflexions of the P'' structure have only one or two contributions and might provide useful information since the structure factors of these reflexions show large variations. Lattice imaging is another method for selecting the correct model because the projection of the clusters along special directions will appear quite different both in size and shape. The present difficulty is that the resolution must be improved to about 2 Å.

Although no conclusive evidence for one model can

be given, the $\frac{1}{2}\langle 111\rangle_c$ type appears preferable because the fit to observed structure factors is better, the bonding of the tetrahedra resembles the bonding in Fe_3O_4 and stresses can apparently be well relieved. The existence of free vacancies in $\frac{1}{2}\langle 100\rangle_c$ models is not favoured if vacancies are stabilized by the interstitials, but on the other hand, proposed diffusion mechanisms make use of free vacancies (Greenwood & Howe, 1972).

Through the present study a different lattice symmetry for the ordered superstructure and a lower point symmetry of the cluster than in previous investigations, are found.

The authors are grateful to Dr J. K. Gjønnes for valuable discussions of the present work.

References

ANDERSON, J. S. (1970). In *Problems of Nonstoichiometry*, edited by A. RABENAU. Amsterdam: North Holland.
CAHN, J. W. (1968). *Trans. AIME*, **242**, 1037–1045.
CHEETMAN, A. K., FENDER, B. E. F. & TAYLOR, R. I. (1971). *J. Phys. C: Solid State Phys.* **4**, 2160–2165.
DARKEN, L. S. & GURRY, R. W. (1945). *J. Amer. Chem. Soc.* **67**, 1398–1412.
FENDER, B. E. F. & RILEY, F. D. (1969). *J. Phys. Chem. Solids*, **30**, 793–798.
GREENWOOD, N. N. & HOWE, A. T. (1972). *Proc. 7th Int. Symp. Reactivity of Solids, Bristol*, pp. 240–251.
HAYAKAWA, M., COHEN, J. B. & REED, T. B. (1972). *J. Amer. Ceram. Soc.* **5**, 160–164.
HAYAKAWA, M., MORINGA, M. & COHEN, J. B. (1974). *Defects and Transport in Oxides*, edited by M. S. SELTZER & R. I. JAFFEE, pp. 177–204. New York: Plenum.
HENTSCHEL, B. (1970). *Z. Naturforsch.* **25a**, 1996–1997.
HERAI, T. & MANENC, J. (1964). *Mém. Sci. Rev. Métal.* **61**, 677–686.
HERAI, T., THOMAS, B., MANENC, J. & BÉNARD, J. (1964). *C. R. Acad. Sci. Paris*, **258**, 4528–4530.
HOANG, C. T., ROMANOV, A. D., SHAYOVICH, YA. L. & ZVINCHUK, R. A. (1973). *Vestn. Leningr. Univ. Ser. Fiz. Khim.* **4**, 144–149.
IIJIMA, S. (1974). *Diffraction Studies of Real Atoms and Real Crystals*, pp. 217–218. Australian Academy of Science.
JANOWSKI, J., JAWOSKI, M. & BENESCH, R. (1973). *Arch. Eissenhüttenwes.* **44**, 721–725.
KOCH, F. & COHEN, J. B. (1969). *Acta Cryst.* B**25**, 275–287.
KOFSTAD, P. & HED, A. Z. (1968). *J. Electrochem. Soc.* **115**, 102–104.
MANENC, J. (1968). *Bull. Soc. Fr. Minér. Crist.* **91**, 594–599.
MORRAL, J. E. & CAHN, J. W. (1971). *Acta Metall.* **19**, 1037–1045.
ROTH, W. L. (1960). *Acta Cryst.* **13**, 140–149.
SMUTS, J. (1966). *J. Iron St. Inst.* **204**, 237–239.
VALLET, P. & RACCAH, P. (1965). *Mém. Sci. Rev. Métall.* **62**, 1–29.

Acta Cryst. (1977). A**33**, 276–279

X-ray Diffraction and Transmission Electron Microscopy Study of Extremely Large-Period Polytypes in SiC

BY M. DUBEY AND G. SINGH

Department of Physics, Faculty of Science, Banaras Hindu University, Varanasi – 221005, *India*

AND G. VAN TENDELOO

Rijksuniversitair Centrum Antwerpen, Middelheimlaan 1, *B*-2020 *Antwerpen, Belgium*

(*Received* 24 *May* 1976; *accepted* 4 *October* 1976)

Extremely large-period polytypes in SiC have been investigated by single-crystal X-ray diffraction and direct lattice imaging by electron microscopy, which has been found to be a more suitable technique for studying structures of extremely large periodicities. Some crystals giving rise to a diffuse streaking along $h0.l$ reciprocal lattice rows when studied by X-ray diffraction, showed the presence of extremely long-period polytypes when investigated by electron microscopy. The c periodicity of such SiC structures (having periodicities of more than 1000 Å) has been determined by this technique and the super-period block spacing is found to contain block spacings of 6*H*, 15*R*, 4*H* and 21*R* polytypes.

Introduction

A number of substances are known to crystallize in polytypic modifications and SiC is a prominent example of this category. The X-ray diffraction studies show that SiC crystals often possess one-dimensional disorder (Verma & Krishna, 1966). The occurrence of one-dimensional disorder in SiC crystals has been investigated in some detail by electron microscopy (Sato & Shinozaki, 1975), X-ray diffraction and chemical etching techniques (Ram, Dubey & Singh, 1974; Ram & Singh, 1976). The existence of one-dimensional disorder in SiC crystals is inferred from the continuous streaks usually found in single-crystal X-ray diffraction patterns along $h0.l$ reciprocal lattice rows. However it is shown that these streaks can also arise as a result of extremely high c periodicities of the crystals as their $h0.l$ spots cannot be resolved easily (Ram,